Journal of Fluorescence (2019) 29:779–795
https://doi.org/10.1007/s10895-019-02396-y

ORIGINAL ARTICLE

Chlorine (Cl) - Substituted Carbazole Based A-π-D-π-a Push-Pull Chromophores as Aggregation Enhanced Emission (AEE) Active Viscosity Sensors: Synthesis, DFT and NLO Approach

Prerana K. M. Lokhande[1] · Dinesh S. Patil[1] · Mayuri Kadam[1] · Nagaiyan Sekar[1]

Received: 15 March 2019 / Accepted: 28 May 2019 / Published online: 6 June 2019

Abstract

Three new carbazole functionalized A-π-D-π-A extended chromophores **4a**, **4b** and **4c** comprising of different chemical functional groups on C=C bond with the assistance of chlorovinylene group in π-conjugation are synthesized and investigated spectroscopically. We have investigated the effect of different electron acceptors - carboxycyanomethylene, dicyanomethylene and 2-(benzothiazol-2-yl) cyanomethylene, the effect of the insertion of chlorine in π-conjugation on photophysical properties and the effect of double acceptors. The chromophores **4a**, **4b** and **4c** exhibited positive solvatochromism with large Stokes shifts and bright orange to red solid-state fluorescence. Amongst all the three compounds **4c** exhibited maximum emission wavelength at 615 nm in DMSO. They presented characteristic twisted intramolecular charge transfer (TICT) emission. Observations exhibited that **4c** containing long hexyl group in donor unit and 2-(benzothiazol-2-yl) cyanomethylene as an acceptor group formed an aggregate in the mixture of solvents and exhibited better aggregation enhanced emission (AEE) compared to the other two derivatives. Amongst the three styryls, **4c** showed the highest emission intensity 299 a.u. at 90% water:DMF fraction (f_w). Chromophores **4a-4c** also exhibited good fluorescence response towards viscosity. Among the three fluorescent molecular rotors (FMR), **4c** exhibited excellent viscosity sensitivity with x value = 0.687. The Non-linear (NLO) characters are estimated with the help of solvatochromic and computational methods using the functionals, B3LYP and CAM-B3LYP. The dyes showed large "linear polarizability (α_{CT})", "first order hyperpolarizability" (β) and "second order hyperpolarizability" (γ) values which show that synthesized styryls can be used as a "NLO" material. The α_{CT}, β and γ for **4c** are found to be the maximum amongst the all three dyes which can be ascribed to the smaller band gap apparent from experimental as well as DFT method.

Keywords Extended styryl · Solvatochromism · AEE · FMR · DFT · NLO

Introduction

Carbazole moiety is considered as a good electron donor to construct active molecules in numerous fields such as "organic light emitting diodes" (OLED) [1], "dye-sensitized solar cells" (DSSC) [2–3], "non-linear optics" (NLO) [4], photoconductors [5], "solid state lasers" [6], and "bio-imaging" [7] due to its good charge transporting properties with low glass transition temperature (Tg), and by simple substitution of -NH of carbazole moiety with a long alkyl chain affords [8–9] solid-state emission, good spectral properties, and electro-optical properties. Also, the insertion of electron withdrawing groups at 3 and 6 positions of carbazole with regard to the bridging nitrogen leads to effective Intramolecular Charge Transfer (ICT) [10] and it also displays high thermal, morphological, chemical and environmental stability [11–13].

"Aggregation Enhanced Emission" (AEE) active moieties are designed and synthesized to accomplish numerous solid-state luminescent materials [14]. Two representative AEE-active molecules are reported in which one comprises strong ICT states, which assume a twisted geometry in the excited state S_1 in solution [15–16] and other is dependent on propeller-shaped "molecular rotamers", displaying active rotation in dilute solution [17–18] due to the formation of H−/J-

Electronic supplementary material The online version of this article (https://doi.org/10.1007/s10895-019-02396-y) contains supplementary material, which is available to authorized users.

✉ Nagaiyan Sekar
n.sekar@ictmumbai.edu.in; nethi.sekar@gmail.com

[1] Department of Dyestuff Technology, Institute of Chemical Technology, Matunga, Mumbai 400 019, India

aggregates in aggregation state [19], excimer emission [20] or enhancement through H-bonding [21–24]. Such fluorescent molecules are effective chromophores due to their typical ICT characteristics [25]. Fluorescent molecules are extensively studied by researchers to tune their ICT properties to be applicable in different fields. They are widely used in many emergent areas of applications for instance "fluorescent probes" [26–28] "electroluminescence devices" [29], "NLO materials" [30], "organic light-emitting diodes (OLEDs)" [31], "solid-state lasers" [32] and "DSSC" [33]. Though, making such organic AEE materials with an exceptional reversible capacity, and high solid-state fluorescence quantum yield and to explore the relationship between structure and AEE properties is still challenging. Conjugated AEE molecules consisting of organic (D-π-A) systems comprise of donor connected to acceptors via π-bridge [34–35]. The presence of halogen in luminescence phenomena with high quantum yield and good stability can be an essential key factor to design the AEE molecules [36].

Organic NLOphoric materials have attracted a great deal of importance over inorganic materials like lithium niobate due to its fast response time [37–39]. This difference lies in the fact as optical properties of organic NLO material is purely electronic in origin whereas, for inorganic NLO materials, it originates through turbulence in structural arrangements of key ions inside the solid-state crystalline framework [40–42]. Amongst the several organic dyes, the carbazole-based ones, the recognized rigid aromatic dyes, receive great consideration because of their excellent photophysical characteristics, high molar absorptivity, fluorescence quantum yields, and their excellent stability towards chemicals, heat, and light [43]. The peripheral modification of carbazole by varying substituents at 2nd, 3rd, 6th, 7th and 9th position, can enhance the NLO response of push-pull system [44].

Accordingly, herein, we have studied three carbazole mediated A-π-D-π-A type AEE active molecules namely **4a**, **4b**, and **4c**. These AEE active chromophores consist of carbazole as a donor, 1-chlorobuta-1,3-diene as a π-spacer and three different electron withdrawing groups namely carboxycyanomethylene, dicyanomethylene and 2-(benzothiazol-2-yl) cyanomethylene as an acceptor. We have evaluated the effect of structural modulation of molecules with various acceptors on ICT characteristics, fluorescent molecular rotor (FMR) properties, AEE and NLO characteristics of the molecules. We have tried to extend the conjugation by inserting an extra π-bond in charge transfer system to configure their effect on photophysical properties and have introduced additional electron withdrawing chlorine atom in π-spacer to increase the accepting capacity of chromophore as it is observed that ICT stabilizes the π-orbitals facilitating the ionization of electrons from the orbitals of the unshared pairs of chlorine. Also, the presence of halogen atom (−X) in a molecule can give an enhancement in the emission intensity as it shows interactions of C–H——Cl (halogen) which are responsible for the unique J aggregate formation and leads to enhanced aggregation induced emission [45–47]. Molecules **4a-4c** displays AEE phenomenon having emission intensity significantly boosted in the aggregation state as well as the solid state. Further, to investigate the importance of chlorine and structural modification of carbazole chromophore on photophysical properties and AEE characteristics of the molecules, we have carried out a comparative study [48]. Geometrical optimizations were done using the method, B3LYP/6–31 + G(d) [49, 50] and DFT computations are used to estimate the structural, electronic properties of carbazole based molecules and to study the "NLO characteristics" of new generation push-pull colorants.

Experimental Section

Materials and Equipment

All the chemicals were procured from "Sigma Aldrich" and "S. D. Fine Chemicals Pvt. Ltd." Pre-coated silica gel aluminium backed TLC plates were used to monitor the reaction. 1H and ^{13}C NMR spectra were obtained on a "500 MHz Varian, USA instrument" with TMS as an internal standard. Absorption spectra were obtained using "Perkin Elmer Lambda 25 UV-visible spectrophotometer". "Varian Cary Eclipse" fluorescence spectrophotometer was used to record fluorescence emission spectra using dye solution of 1 X 10^{-6} mol L^{-1}. Fluorescence quantum yield was obtained with fluorescein as the reference standard (in 0.1 M NaOH) [51].

Computational Strategy

DFT and TD-DFT calculations were applied for comparing the observed absorption values. The method was applied to study the structural modification in compounds and to relate its effect on photophysical properties. DFT method was used for geometry optimization in ground state (S_0). All the calculations were achieved with "Gaussian 09 package" [52]. The hybrid functional namely "B3LYP (Becke3-Lee-Yang-Parr hybrid functional)" was used. B3LYP [53] method used for the vibration frequency of each compound computed using TD-DFT calculation at 6–31 + G(d) basis set. The TD-DFT calculation used for the optimization of the structure at first singlet excited state (S_1) of each molecule with its minimum energy geometry [54–57]. The "Polarizable Continuum Model" (PCM) [58, 59] was applied for S_0 and S_1 state geometry optimization in solvent. The solvents used were toluene, chloroform ($CHCl_3$), ethanol (EtOH), dimethyl sulfoxide (DMSO).

The NLO characters of chromophores were estimated by solvatochromic as well as computational methods. The

"polarizability parameter" a_{CT}, "first hyperpolarizability parameter" β_{CT} and "second hyperpolarizability" γ were calculated by solvatochromic two level microscopic model and DFT method.TD-DFT functionals namely, "B3LYP and CAM-B3LYP" were used to calculate NLO parameters.

Synthesis and Characterization

The synthetic route of intermediates **1**,**2**,**3**, and target compounds **4a**,**4b** and **4c** are showed in Scheme 1.

9-Hexyl-Carbazole (1)

To a solution of 9-H-carbazole (1 g, 5.9 mmol) in acetone (20 mL) was added KOH (0.66 g, 11 mmol) and stirred the mixture for 2 h at room temperature. 0.83 mL of 1-bromohexane (0.98 g, 59 mmol) was then added to the above mixture and refluxed it for 24 h. After the complete consumption of starting material (confirmed by TLC), the solvent was removed under reduced pressure. 50 mL H_2O was then added to the solution and obtained solid was filtered followed by recrystallization using EtOH and water to give colourless solid (0.8 g, yield 80.0%).

3,6-Diacetyl-9-Hexyl-Carbazole (2)

To a solution of 9-hexyl-carbazole (0.8 g, 3.1 mmol) in chloroform (10 mL) was slowly added anhydrous $AlCl_3$ (1.27 g, 9.56 mmol) with constant stirring under cooling condition. After cooling to 0 °C, 0.67 mL of acetyl chloride (0.74 g, 9.48 mmol) in 10 mL of chloroform was added dropwise over 10 min under vigorous stirring and stirring continued for 3–4 h at ambient temperature. The reaction mixture was neutralized and then extracted with DCM twice, washed by 1 M $NaHCO_3$ and water. The organic phase was dried over anhydrous $MgSO_4$. The organic layer was completely removed under reduced pressure and the crude solid obtained was then purified by column chromatography using petroleum ether and ethyl acetate (9:1) as eluent to give the desired compound (0.7 g, 80%).

^{1}H NMR (500 MHz, $CDCl_3$) δ 8.77 (d, J = 1.6 Hz, 2H), 8.16 (dd, J = 8.6, 1.7 Hz, 2H), 7.44 (d, J = 8.7 Hz, 2H), 4.32 (t, J = 7.3 Hz, 2H), 2.73 (s, 6H), 1.84–1.90 (m, 2H), 1.39–1.24 (m, 6H), 0.84 (t, J = 7.1 Hz, 3H).

^{13}C NMR (125 MHz, $CDCl_3$) δ 197.48, 143.87, 129.66, 126.98, 122.86, 122.00, 108.97, 43.61, 31.44, 28.88, 26.84, 26.68, 22.47, 13.96.

3-Chloro-3-(6–1-Chloro-3-Oxoprop-1-en-1-Yl) -9-Hexyl-9H-Carbazol-3-Yl)Acrylaldehyde (3)

To anhydrous DMF in a round bottom flask, phosphorus oxychloride ($POCl_3$, 4.4 mmol) was added dropwise at 0 °C and stirring continued for another 30 min then added solution of compound **2** (0.5 g, 1.49 mmol) in anhydrous DMF. Then the mixture was heated to 70 °C for 2 h. The solution was then rapidly transferred into cold water and neutralized with $NaHCO_3$ followed by extraction with ethyl acetate (20 mL)

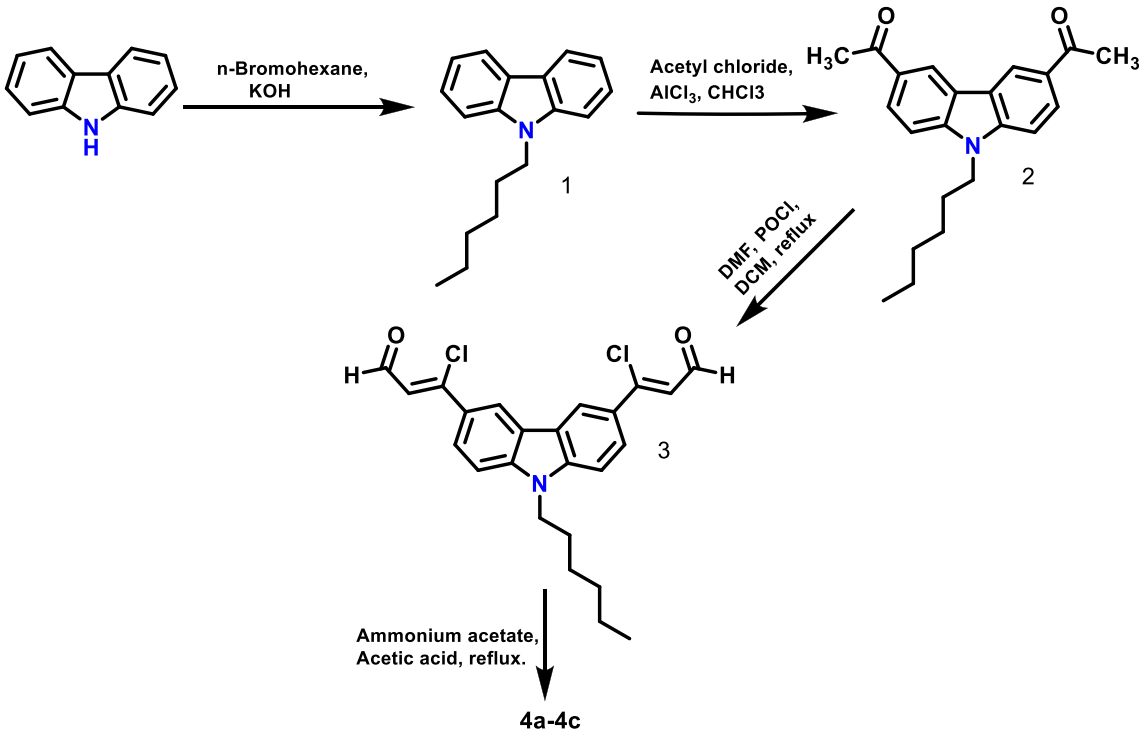

Scheme 1 Synthetic pathway for the synthesis of molecules **4a-4c**

and the organic layer was then dried over anhydrous $MgSO_4$. The organic layer was concentrated and the crude solid obtained was purified by column chromatography (neutral alumina; ethyl acetate/petroleum ether,1/10, *v*/v) to provide a yellow solid (0.42 g, yield: 85%).

5-(6–4-Carboxy-1-Chloro-4-Cyanobuta-1,3-Dien-1-Yl) -9-Hexyl-9H-Carbazol-3-Yl) -5-Chloro-2-Cyanopenta-2,4-Dienoic Acid (4a)

To a solution of intermediate **3** (0.2 g, 0.46 mmol) in 10 mL MeOH, was added cyanoacetic acid (0.087 g, 1 mmol), ammonium acetate (0.03 g). Acetic acid was added to the solution in catalytic amount (1–2 drops). The solution was refluxed for 18 h. After cooling down to room temperature, the solvent was removed by rotary evaporation. The crude product was obtained by silica gel chromatography (CH_2Cl_2: MeOH, 95:5 as eluent) as a dark red solid. Yield: 77%.

^{1}H NMR (500 MHz, DMSO) δ 8.90 (d, J = 1.8 Hz, 1H), 8.16 (d, J = 11.4 Hz, 1H), 7.97 (dd, J = 8.8, 1.8 Hz, 1H), 7.76 (d, J = 8.9 Hz, 1H), 7.33 (d, J = 11.4 Hz, 1H), 4.45 (t, J = 6.6 Hz, 2H), 1.76 (dd, J = 12.8, 6.0 Hz, 2H), 1.35–1.09 (m, 6H), 0.78 (t, J = 7.1 Hz, 3H).

^{13}C NMR (125 MHz, DMSO) δ 172.43, 163.40, 146.34, 142.77, 127.74, 126.31, 122.87, 121.58, 119.24, 116.94, 110.88, 43.31, 31.34, 28.93, 26.44, 22.41, 14.28.

CHN analysis: Calculated C, 64.06; H, 4.48; Cl, 12.61; N, 7.47; **Found** C, 64.07; H, 4.4; N, 7.47%.

2,2′-(9-Pentyl-9H-Carbazole-3,6-Diyl) Bis(3-Chloroprop-2-en-3-Yl-1-Ylidene))Dimalononitrile (4b)

To a solution of intermediate **3** (0.2 g, 0.46 mmol) in 10 mL MeOH, was added malononitrile (0.077 g, 1 mmol), ammonium acetate (0.03 g). Acetic acid was added to the solution in catalytic amount (1–2 drops). The solution was refluxed for 18 h. After cooling down to room temperature, the solvent was removed by rotary evaporation. The product was obtained by silica gel chromatography (CH_2Cl_2: MeOH, 95:5 as eluent) as a dark red solid. Yield: 80%.

^{1}H NMR (500 MHz, $CDCl_3$) δ 8.66 (d, J = 0.7 Hz, 1H), 8.15 (dd, J = 11.5, 1.0 Hz, 1H), 8.00 (dd, J = 8.3, 1.3 Hz, 1H), 7.51 (d, J = 8.8 Hz, 1H), 7.42 (dd, J = 11.5, 0.9 Hz, 1H), 4.39 (t, J = 7.1 Hz, 1H), 1.92 (dt, J = 14.6, 7.2 Hz, 1H), 1.43–1.26 (m, 4H), 0.88 (t, J = 6.8 Hz, 2H).

C 68.72, H 4.43, N 13.36.

^{13}C NMR (125 MHz, $CDCl_3$) δ 155.74, 155.28, 155.01, 151.88, 143.54, 142.92, 128.40, 127.31, 127.12, 126.74, 126.57, 123.19, 122.98, 122.85, 122.77, 121.75, 117.90, 117.84, 113.73, 112.10, 110.05, 83.32, 43.93, 31.42, 28.96, 26.85, 22.47, 13.96.

CHN analysis: Calculated: C, 68.71; H, 4.42; N, 13.35%. **Found**: C, 68.72; H, 4.43; N, 13.36%.

5,5′-(9-Hexyl-9H-Carbazole-3,6-Diyl) Bis(2-(Benzo[d] Thiazol-2-Yl)-5-Chloropenta-2,4-Dienenitrile) (4c)

To a solution of intermediate **3** (0.2 g, 0.46 mmol) in 10 mL MeOH, was added 2-(benzothiazol-2-yl) acetonitrile (0.085 g, 1 mmol), ammonium acetate (0.03 g). Acetic acid was added to the solution in catalytic amount (1–2 drops). The solution was refluxed for 18 h. After cooled down to room temperature, the solvent was removed by rotary evaporation. The product was obtained by silica gel chromatography (CH_2Cl_2: MeOH, 95:5 as eluent) as a dark red solid. Yield: 84%.

^{1}H NMR (600 MHz, DMSO) δ 8.25 (d, J = 7.8 Hz, 9H), 7.98 (s, 5H), 7.65 (d, J = 8.3 Hz, 8H), 7.56–7.49 (m, 13H), 7.28–7.24 (m, 8H), 7.18 (d, J = 7.5 Hz, 7H), 6.71–6.66 (m, 10H), 6.44 (d, J = 8 Hz, 10H), 6.34 (d, J = 7.9 Hz, 9H), 6.24–6.18 (m, 11H).

CHN analysis: Calculated: C, 68.10; H, 4.22; N, 9.45. **Found**: C, 68.13; H, 4.23; N, 9.46%.

Results and Discussions

Design and Synthesis

To further explore the application of AEE molecules, we have synthesized three new AEE styryls through a multistep reaction route. All the molecules were synthesized in the multistep synthetic pathway as shown in Scheme 1. Carbazole was first alkylated using n-bromohexane in acetone and KOH, to give N-hexyl carbazole **1**. Further, N-hexyl carbazole was acylated by "Friedel Craft acylation" using acetyl chloride and $AlCl_3$ to give compound **2**. Acylated compound **2** after "Vilsmeier–Haack formylation" gave compound **3** which finally subjected to "Knoevenagel condensation" with various active methylene derivatives, in the presence of NH_4OAc and CH_3COOH to produce styryl dyes **4a-4c** in good yields. Molecular structures of the styryls **4a-4c** are represented in Fig. 1 where highlighted part shows different functionalities introduced on the designed molecule**.**

Photophysical Properties

Styryls **4a**, **4b**, and **4c** possess the molecular structures with different electron withdrawing groups as an acceptor. The optical properties of 1×10^{-6} mol L^{-1} solution of 4a-4c in solvents of different polarities were studied and the corresponding photophysical data are listed in Table 1 and Table S1 (ESI). We have investigated the spectroscopic properties in seven organic solvents of different polarity and proticity: toluene (TOL), ethyl acetate (EA), chloroform ($CHCl_3$), ethanol (EtOH), acetonitrile (CAN), dimethylformamide (DMF) and dimethyl sulfoxide (DMSO). Typical absorption spectra of compound 4c in several solvents is represented in Fig. 2(a)

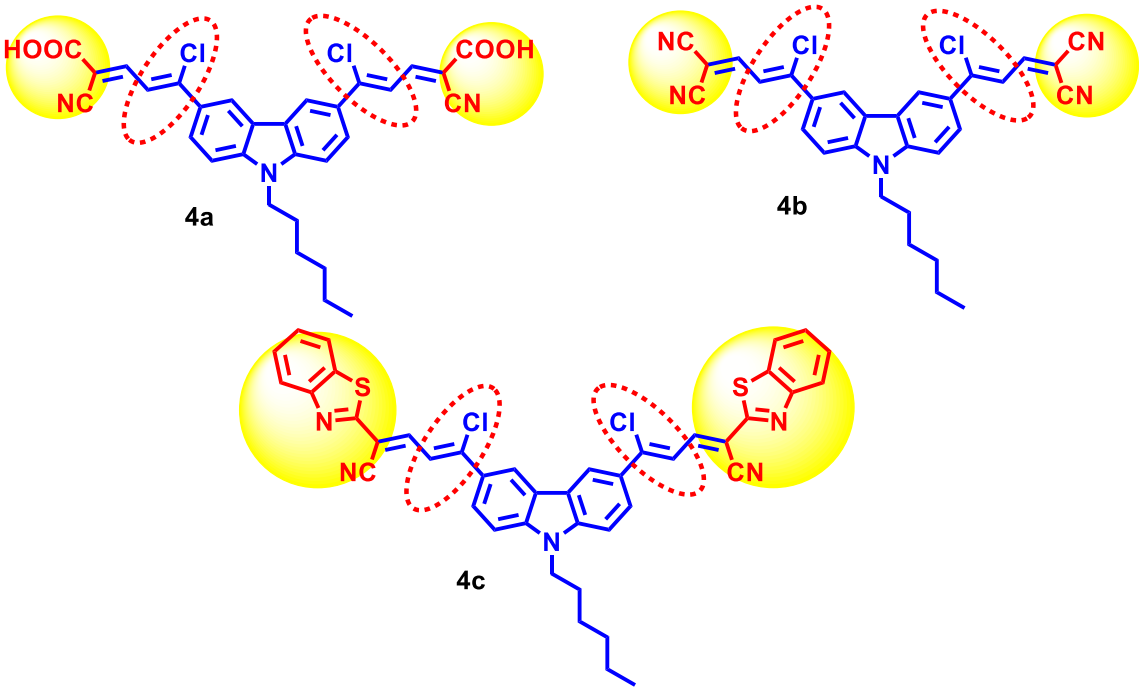

Fig. 1 Molecular structures of chromophores **4a-4c**

and data are recorded in Table 1. Absorption and emission graphs of 4a and 4b are presented in Fig. S1 and data are provided in Table S1. Absorption graphs of compounds 4a-4c presented shorter maxima at around 300–380 nm arising from the π-π* transition and longer and broad maxima at around 400–450 nm owing to ICT between the donor carbazole unit and the electron withdrawing acceptor units. These graphs also showed a shoulder peak at around 460–540 nm, which might be because of conjugation from both the sides of 3 and 6 positions of carbazole. Styryls **4a** and **4b** exhibited higher absorption maxima at 412 nm and 456 nm respectively in DMSO and lower absorption maxima at 387 nm and 435 nm respectively in toluene. From toluene, the absorption maxima of **4c** located at 425 nm start shifting gradually with increasing solvent polarity, and finally reaches 439 nm in DMSO (Fig. 2a, Table 1). Similar observations were seen in

Table 1 Photophysical data of **4c** in several solvents

Dye	Solvent	λ_{abs} [a]	λ_{emi} [b]	Stokes shift (Δv)		ε_{max} [c]	Φ [d]	f [e]	FWHM [f]	σ [g] (10^-19)	μ_{ge} [h]
				nm	cm^{-1}				cm^{-1}	cm^2	Debye
4c	Toluene	425	535	111	4861	38,595	0.324	1.34	15,782	1.47	8.03
	EA	426	540	114	4967	38,518	0.088	1.35	15,783	1.47	8.04
	CHCl3	435	565	130	5479	36,408	0.084	1.19	14,969	1.39	7.5
	Ethanol	429	585	156	6216	38,945	0.076	1.43	14,924	1.48	8.45
	ACN	432	578	146	5856	51,202	0.089	1.83	15,010	1.95	9.99
	DMF	433	600	167	6428	42,349	0.091	1.54	15,306	1.61	8.92
	DMSO	439	615	176	6518	43,203	0.092	1.59	15,512	1.65	9.19

[a] "Maximum absorption wavelength" in nm

[b] "Maximum emission wavelength" in nm

[c] "Molar extinction coefficient" in $Lmol^{-1}$ cm^{-1}

[d] "Fluorescence quantum yield" (estimated using fluorescein as the standard in 0.1 M NaOH)

[e] "Oscillator strength" experimental

[f] "Full width half maxima" of the absorption band

[g] "Molar absorption cross section" in (10^{-19} cm^2)

[h] "Transition dipole moment"

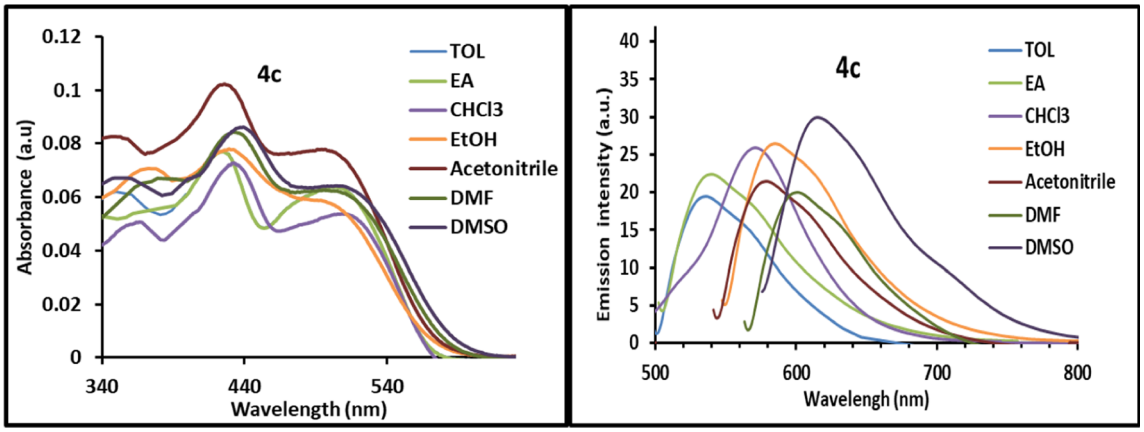

Fig. 2 **a** Typical absorption spectra of **4c** in several solvents. **b** Typical emission spectra of **4c** in several solvents

the case of **4a** and **4b**. The "molar absorptivity (ε)" of **4a-4c** in DMSO were found to be 39,235 $Lmol^{-1}$ cm^{-1}, 28,298 $Lmol^{-1}$ cm^{-1} and 43,203 $Lmol^{-1}$ cm^{-1} respectively.

Compared to absorption wavelength, the emission wavelengths (λ_{emi}) exhibited significant red-shift with the rising polarity of solvents. For example, λ_{emi} of **4c** is 615 nm in polar DMSO, which is red shifted by about 80 nm from that in non-polar toluene (535 nm) (Table 1) (as represented in Fig. 2b). Similarly, λ_{emi} of **4b** slowly red-shifted from non-polar toluene (506 nm) to polar DMSO (570 nm) and the λ_{emi} of **4a** red shifted from (511 nm) toluene to DMSO (564 nm) (Table S1). Amongst all three styryls **4a-4c**, styryl **4c** exhibited highest emission maxima at 615 nm in DMSO owing to the existence of stronger electron withdrawing group 2-(benzothiazol-2-yl) cyanomethylene. With the increasing electron withdrawing capacity, emission wavelength red shifted as following order **4a < 4b < 4c** in DMSO. With the increase in solvent polarity, Stokes shift of **4c** showed an increasing tendency from toluene (4861 cm^{-1}) to DMSO (6518 cm^{-1}) (Table 1). Similar results were obtained for compounds **4a** and **4b** (Table S1). The Stokes shifts are maximum in the polar solvent and can be ascribed to the more stabilized excited state in a polar solvent than non-polar solvents which is responsible for charge transfer. All the compounds **4a-4c** showed positive solvatochromism.

To figure out the basis of the red shifted emission wavelength of **4c**, we further compared the results with the similar derivatives (Table S2, ESI) considering following points: (1) comparison with the similar analogue **R1** with ethyl chain in a donor [48] to investigate the donating capacity of the molecule; (2) comparison with the molecule **R1** [48] without chlorovinylene group to verify the importance of the presence of -Cl substituent; (3) comparison with **R2** having single acceptor (D-π-A) (synthesis is provided in ESI) instead of double acceptors to study the effect of double electron withdrawing groups on the emission. Generally, the extension of π-conjugation and the increased capacity of donor and acceptor groups are effective in enhancing the photophysical properties of compounds. For instance, we compared the photophysical properties of **4c** with previously reported **Dye R1** (Fig. S2), where **R1** with ethyl group on a donor carbazole exhibited (λ_{abs}) at 420 nm and (λ_{emi}) at 505 nm in DMF whereas synthesized **4c** with hexyl group on carbazole, additional π-bond in conjugation and electron withdrawing chlorine group showed λ_{abs} at 433 nm and λ_{emi} at 600 nm in DMF due to the elongation of conjugate chain and increased electron donating and accepting capacity of molecule. The designed synthetic strategy furnished a red shift of about 13 nm in absorption maxima and 95 nm in emission maxima. Stokes shift also showed an increment from 4008 cm^{-1} **(R1)** to 6428 cm^{-1} **(4c)** Table S2(a). So, the presence of chlorine with an additional π-bond helped to increase the conjugation length and the accepting capacity of chromophore and facilitates the ionization of electrons from the orbitals of the unshared pairs of chlorine which can be responsible for a bathochromic shift in absorption along with the emission wavelength. Further, we investigated the importance of double acceptors by comparing with **R2** (single acceptor) (Fig. S2 Table S2(a)), where **R2** showed (λ_{abs}) at 430 nm and λ_{emi} at 591 nm in DMF whereas an enhancement was observed in case of **4c** due to the presence of double acceptors and increased conjugation length Table S2(a). We have also compared the results of 4c with other similar reported analogues [105, 106] Table S2(b), where compound **4** with $-NO_2$ as an acceptor showed λ_{abs} at 363 nm and λ_{emi} at 585 nm, compound **5** showed λ_{abs} at 301 nm and λ_{emi} at 397 nm and **CS3** showed λ_{abs} = 434 nm, λ_{emi} = 504 nm in chloroform while the designed strategy of the present paper resulted in longer absorption and emission wavelength (for **4c**, λ_{abs} = 425 nm, λ_{emi} = 535 nm) due to the presence of hexyl group in a donor, chlorine group with an additional π-bond in the conjugation and stronger withdrawing acceptor group.

All three compounds exhibited solid-state emission around 450–700 nm represented in Fig. 3. **4a-4c** showed a bathochromic shift in solid state absorption and emission wavelength compared to their absorption and emission in the

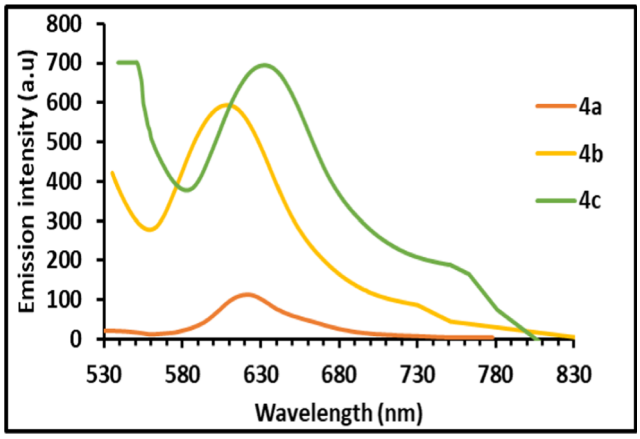

Fig. 3 Solid-state emission graph of **4a-4c**

solution state. The compounds **4a**, **4b** and **4c** exhibited increased emission intensity in a solid state which is around 95 a.u, 589 a.u and 685a.u respectively. Also, **4a-4c** showed red shifted emission wavelength in a solid state because of the aggregate formation in the solid state. With the increase in solvent polarity, fluorescence quantum yield decreases from non-polar solvent to polar solvent [60–63]. The extended styryl **4c** gave $\phi = 0.324$ and $\phi = 0.076$ in toluene and ethanol respectively Table 1. **4b** showed similar results, where it exhibited maximum quantum yield in toluene ($\phi = 0.298$) and minimum quantum yield in ethanol (0.061) (quantum yields are measured using quinine sulfate as a standard [61–63]) Table S1.

Above discussion indicates that 2-(benzothiazol-2-yl) cyanomethylene can be a better acceptor compared to the other two electron withdrawing groups. Further the designed strategy of increasing the conjugation length, increasing the electron donating and accepting capacity by substituting ethyl with hexyl group in a donor, using double acceptors and inserting chlorine group with an additional π-bond in the conjugation between donor and acceptor furnished bathochromic shift in the solution and the solid-state emission both.

Oscillator Strength and Transition State Dipole Moment

"Oscillator strength" explains about the probability of spectral characteristics in energy levels. It provides information about intramolecular charge transfer. It can be estimated using the following Eq. 1

$$f = 4.32 \times 10^{-9} \ \varepsilon\,(\nu)\, d\nu \qquad (1)$$

From the value of "***f***", transition dipole moment can be estimated, which is the difference in electric charge distribution between the S_0 and S_1 state of the compound [64, 65]. The increase in the oscillator strength results into increased transition dipole moment. Styryl **4c** exhibited an enhancement in transition dipole moment with increasing oscillator strength Table 1. The styryls showed a range of transition dipole moment as follows: **4a** (6.88–7.68 D), **4b** (6.41–7.91 D) and **4c** (7.50–9.99 D) which conclude that styryl **4c** exhibits better charge transfer than other two derivatives owing to the stronger electron acceptor in **4c**.

Polarity Plots and Dipole Moment Ratio

We have examined the photophysical character of the A-π-D-π-A carbazole styryls to investigate the role of strong electron accepting groups and the effect of extended conjugation on the ground and excited-state characteristics. Dyes **4a-4c** showed red shifts in CT absorption band by varying solvent polarity from toluene to a DMSO solvent, signifying the highly stabilized S_1 than the S_0 state. Further, dipole moment ratios were estimated using Bilot-Kawski [64, 65] and Bakhshiev [66–68] functions plots for **4a-4c** and are presented in Table S3. The increase in Stokes shift for compounds 4a-4c with rising solvent polarity is ascribed to the polarized excited state (S_1) in the polar microenvironments. The ratio of μ_e/μ_g for dyes **4a-4c** is found to be more than unity representing higher polarity of the S_1 state dipole moment than the S_0 state dipole moment, resulting in the charge transfer in the S_1 state. A change in a solvent polarity, dielectric constant and polarizability of the medium affects the ground and excited state.

We plotted graph of Stokes shifts Vs the "solvent orientation polarizability", the respective "Lippert-Mataga plots" [69] are shown in Fig. 4. The observed linearity proposed that a single S_1 state was present on excitation. The slope of the "Lippert-Mataga plots" of all the three dyes proposed a higher contribution of the S_1 dipole moment than the dipole moment in S_0. The upgraded form of "Lippert-Mataga model" i.e. "McRae [70] function (f_{McRae})" vs Stokes shift in cm^{-1} was plotted which gave a linear relationship with a good regression coefficient for **4a**-4c (Fig. S3). Hence, the difference in the dipole moment of S_1 and S_0 states evaluates the CT characteristic of the compounds [71, 72].

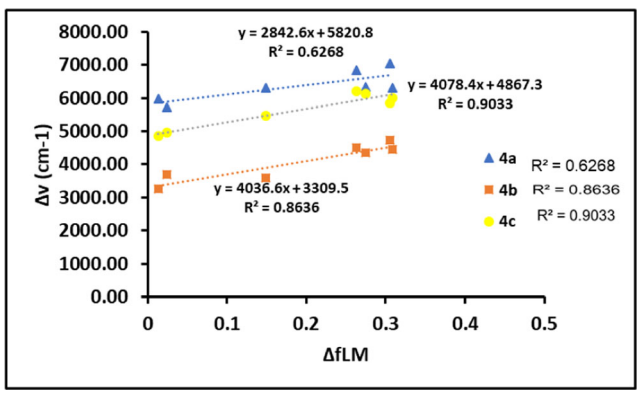

Fig. 4 Lippert-Mataga plots of **4a-4c**

"Weller equation" can be used to get a more quantifiable investigation of the fluorescence solvatochromism [73]. "Weller equation" is an upgraded form of the "Lippert-Mataga equation", helps to calculate the dipole moment of the S_0 state (μ_e). In the "Weller plot" [Fig. S4], the observed regression coefficients are 0.5754, 0.8606 and 0.9059 for the dyes **4a-4c** respectively this shows that the molecules exhibit more CT properties in the S_1 state. To understand more about the S_1 state that whether **4a-4c** are showing ICT characteristics or TICT, we used "Rettig equation", a plot of $\Delta\bar{\upsilon}_{emi}$ (cm^{-1}) vs "Rettig function" [74, 75] [Fig. S5]. All the molecules **4a-4c** exhibited a linear relationship from non-polar to polar solvents and the regression coefficients were obtained as 0.5806, 0.8604 and 0.9090 for **4a-4c** respectively. From the observations, it can be confirmed that all the molecules show more or less TICT but **4c** has the highest regression coefficient than **4a** and **4b** and it shows more TICT properties.

Aggregation Enhanced Emission (AEE)

The "AEE" characteristics of the styryls **4a**, **4b** and **4c** were examined in a mixture of DMF and H_2O (Fig. 5 (a-b)). All the three styryls **4a-4c** were well-dispersed in DMF and presented fluorescence emission with weak intensity in their solution state. To examine the AEE activity of **4a-4c**, emission graph of dyes was investigated in a sequence of mixtures of H_2O–DMF with different water fractions (f_w). As H_2O is the anti-solvent for the dyes, the increase in H_2O fraction changes the solution form into aggregated particles in the mixture of DMF and H_2O. The concentration was maintained at 1×10^{-6} mol L^{-1}. We observed the transition in the λ_{emi} and fluorescence intensity by gradually adding water fractions (f_w) of 0–90% to the pure DMF solutions. Till the water fraction 40%, the only slight increase was observed in fluorescent intensity but with the further increase in water fraction from 50% onwards, **4a-4c** showed dramatic increment in the fluorescence intensity showing bright orange luminescence under UV radiation. Figure 5(a) and Fig. S6 reveals that dyes **4a-4c** display higher fluorescence intensity at water fraction (f_w) 90%. It is remarkable that with steady addition of water fraction to the solution of dye **4c** in DMF, the emission wavelength was red shifted to 632 nm when f_w was between 50 and 90 vol%.

Similar observations were noticed for the **4a** and **4b** styryls. The emission intensity of styryl **4c** found to be the highest when water fractions (f_w) was 90%. In the case of **4b**, emission wavelength increased gradually and showed dramatic red shit after 70% water fraction. Similarly, emission intensity also showed maximum enhancement after 70% water fraction. **4b** exhibited highest emission wavelength and fluorescence intensity at water fraction (f_w) 90%. Amongst the three styryls, **4c** showed the highest emission intensity 299 a.u. at 632 nm. So, dyes **4a-4c** are found to be AEE active which is advantageous to find an application in the "fluorescent probe "and in "electroluminescent devices"**.** The red shifted emission peaks of styryls **4a-4c** with rising water fraction may be the result of strong electronic interaction through the π-stacking in aggregate formation and supramolecular interactions of C–H——Cl (halogen) resulting into J aggregate formation [45–47].

Fluorescent Molecular Rotor (FMR) Properties

The effects on the emission intensity with the change in viscosity of solvent for synthesized FMRs **4a-4c** was studied. Thus, these molecules were solubilized in EtOH and viscosity was increased using polyethylene glycol 400 (PEG:400). As the viscosity of the solvent was increased, it resulted in enhanced emission intensities. The effect of the change in

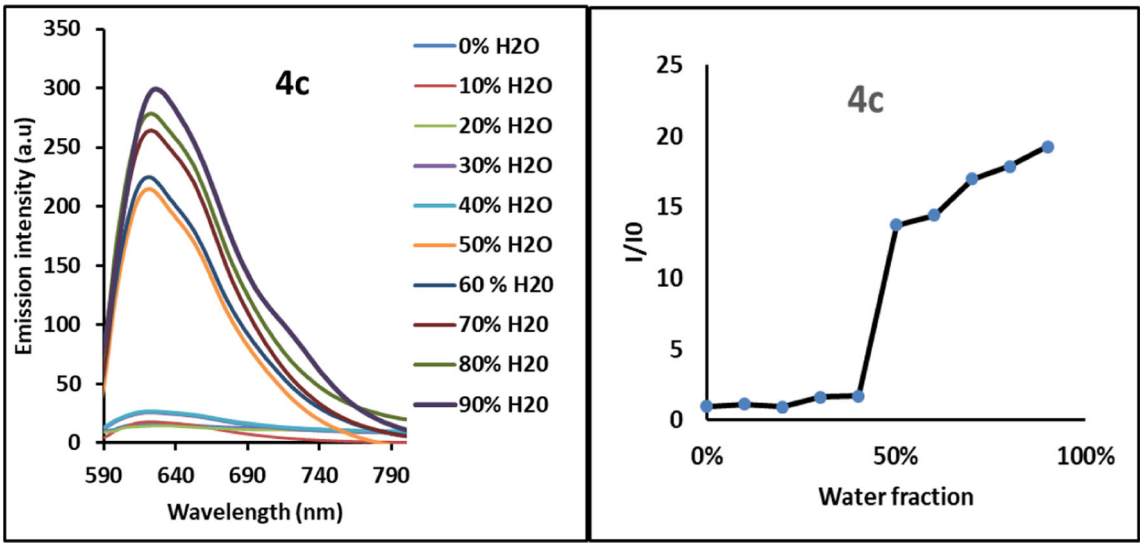

Fig. 5 **(a)** Emission spectra of **4c** in DMF and different H_2O–DMF mixtures**. (b)** Plot of water fraction versus ratio metric fluorescence intensity of **4c** in DMF and water–DMF mixtures

viscosity of solvent on emission intensity of FMR can be explained by using "Forster-Hoffmann" Eq. (2).

$$\log I = C + x \log \eta \quad (2)$$

where.

I emission intensity of FMR
x sensitivity towards viscosity
η viscosity of the mixture

In a low viscous medium the molecules show free movements along the carbon-carbon single and double bond but with an increase in viscosity, free movements along the bonds get prohibited. In a medium of low viscosity, molecules exhibit S_1 state relaxation via "non-radiative pathway" [76, 77] due to the free movements. While in a medium of high viscosity molecules show "restriction of rotation" (RIR) [78] and relaxation proceeds by improved fluorescence emission. The FMRs **4a-4c** exhibited a red shift in emission wavelength as well as emission intensity. With the gradual increase in viscosity of the mixture, the FMRs showed a hyperchromic shift in emission intensity. Figure 6 (a) shows emission graph of **4c** in the mixture of EtOH and PEG 400**.** Amongst all the FMRs, **4c** exhibited a drastic change in emission intensity after 10% PEG 400 and ethanol mixture. Maximum emission intensity for **4c** is 680 a.u. at 90% PEG 400 and ethanol mixture. We have plotted a graph of log I vs log η to calculate the value of x for 4c [Fig. 6 (b)]. Higher the value of x, higher is the sensitivity of FMR towards viscosity.

The FMRs **4a, 4b** and **4c** have x values 0.22, 0.23 and 0.68 respectively. The extended styryls dye **4c** show better improvement in the emission intensity with the rising viscosity as compared to FMR **4a** and **4b**. Emission graphs of **4a** and **4b** in the mixture of EtOH and PEG 400 and graph of log I vs log η of **4a** and **4b** are provided in Fig. S7(a-b) [SI]. The compound **4c** showed good FMR properties than **4a** and **4b**. The same experiment was carried out in DMSO: Glycerol system but no changes were observed. So, we can say that this change in fluorescent intensity is due to the change in viscosity of the mixture and not due to change in a polarity of the solvent.

Geometry Optimization

DFT and TD-DFT calculations were applied to compare the observed absorption and emission values. The method was applied to study the structural modification in dyes and to relate its effect on photophysical properties. DFT method was applied for the S_0 geometry optimization. The TD-DFT calculation at B3LYP/6–31 + G(d) and CAM B3LYP/6–31 + G(d) basis set used for the optimization of the structure at first singlet S_1 state of each molecule with its minimum energy geometry [79]. Figure 7 shows the optimized molecular geometries of **4a-4c**. The observed bond length and bond angles are presented in Table 2 and Table S4-S5. C-H bond lengths increases from 1.085 A° to 1.095A°. The C-C bond lengths increased from 1.428 to 1.466A°. The O-H, N-C and N ≡ C bond lengths showed values of 0.975 A°, 1.386 A° and 1.163 A° respectively. As per the geometry optimization using B3LYP/6-31G+(d), the dihedral angles indicate that the carbazole and acceptor are planar.

"Vertical Excitation", "Frontier molecular orbitals" (FMOs), "global reactivity descriptors" and "molecular electrostatic potential" (MEP)

Electronic Spectra

TD-B3LYP/6–31 + G(d) and CAM-TD-B3LYP/6–31 + G(d) were employed for vertical excitations of the S_0 state geometries of carbazole dyes **(4a-4c)** in solvents of different polarities. All parameters obtained from the computational study are

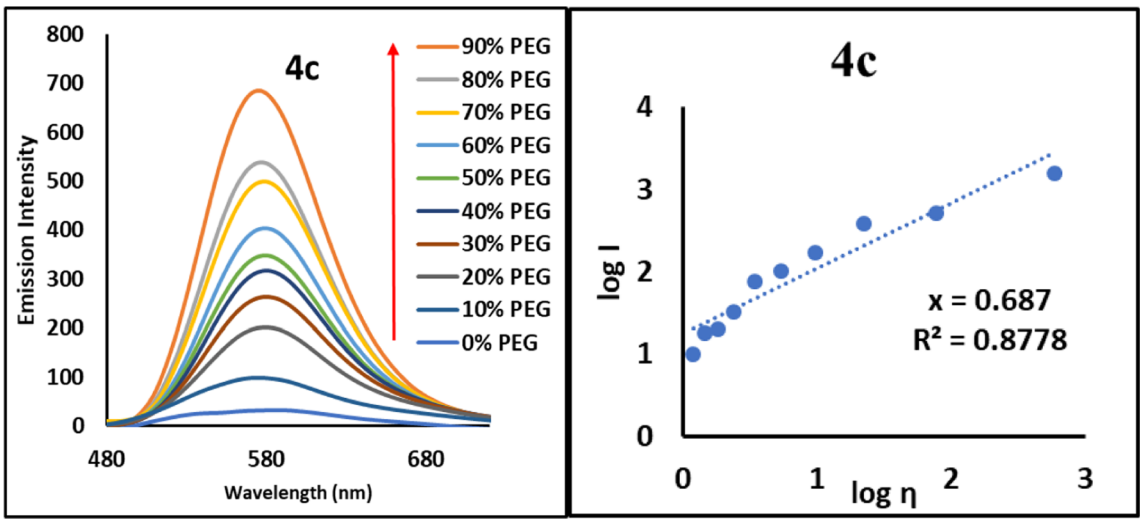

Fig. 6 **a** Emission graph of **4c** in mixture of EtOH and PEG 400**. b** Emission intensity Vs viscosity of solvent for **4c**

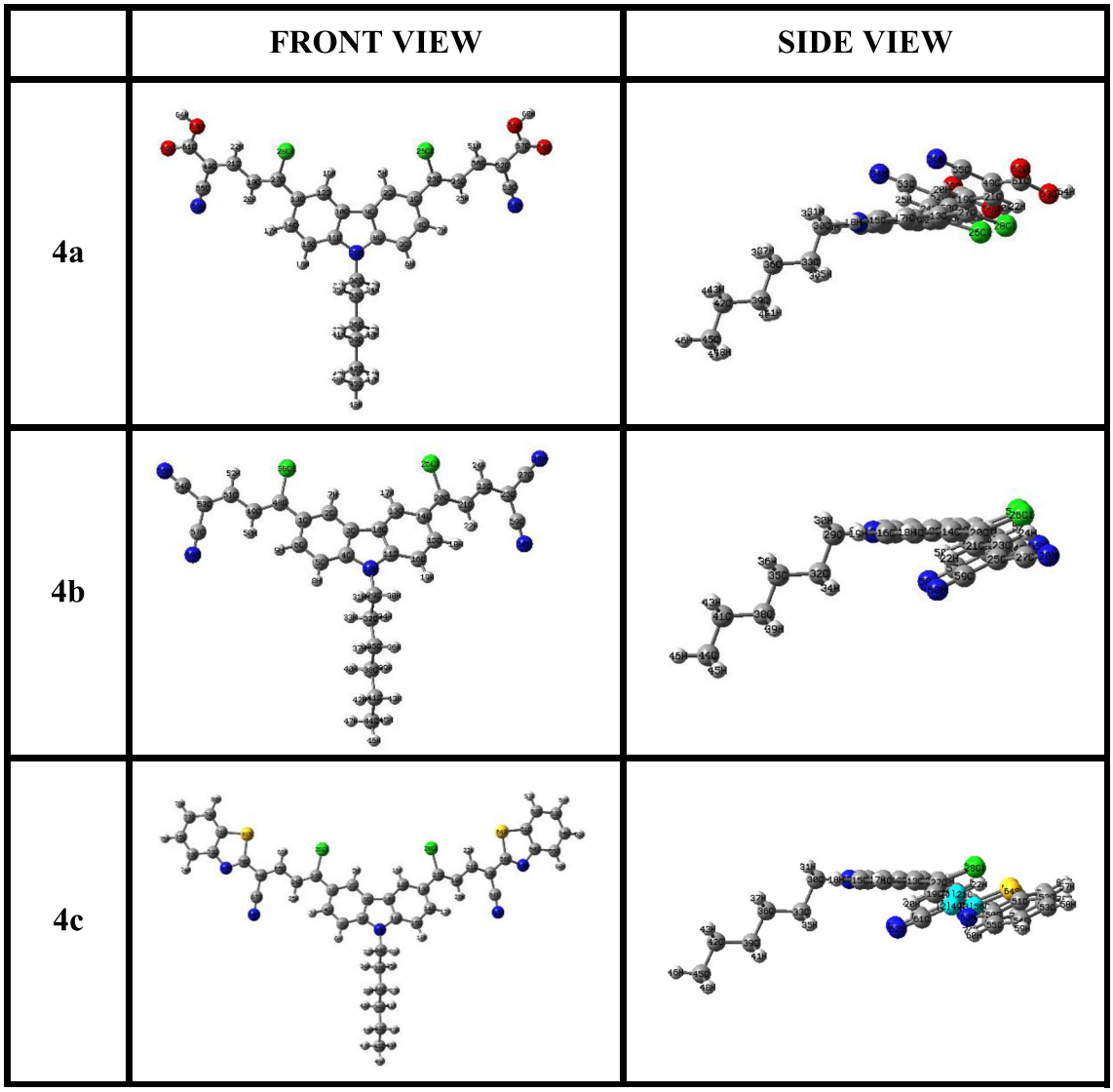

Fig. 7 Optimized geometry of **4a-4c** front view and side view

summarized in Table S6. Dyes **4a-4c** exhibited one shorter wavelength owing to aromatic π-π* transitions. All the dyes exhibited longer absorption peak having higher oscillator strength which can be contributed to the ICT characteristic of dyes. The CT band for **4a-4c** are primarily owing to the transition of an electron from H to L of dyes**.** From TD-B3LYP/6–31 + G(d) basis set, the smaller experimental λ_{abs} for dye **4c** was observed in toluene (425 nm) and maximum in DMSO (439 nm) solvent while the computed smallest vertical excitation is in toluene was (507.86 nm) and highest in DMSO (539.11 nm). For dye **4a** experimental λ_{abs} in toluene (387 nm) and maximum in DMSO (411 nm) solvent however the computed vertical excitation is lowest in toluene (499.06 nm) and maximum in DMSO (520.67 nm). Similar solvatochromism results were obtained for **4b**. Conjugation length is directly proportional to ICT between HOMO and LUMO and the vertical excitations are connected with the HOMO→LUMO transitions and oscillator strength of the compound. Among all the three compounds, **4c** exhibited a maximum oscillator strength and maximum H-L transition contribution.

Homo-LUMO

Usually, the "HOMO" levels are dispersed over donor while the "LUMO" levels are localized on the acceptor. Figure 8 indicates that the "HOMO" levels of **4a-4c** are distributed on carbazole core, and in disparity, the LUMO levels are dispersed on the electron withdrawing unit 2-cyanoacrylic acid, dicyano vinylene and 2-(benzothiazol-2-yl) cyanomethylene. On excitation, electron density population shifts from the carbazole unit to the acceptor moiety. This signifies ICT between donor carbazole and acceptor groups**.** "HOMO–LUMO gaps" in **4a**, **4b**, and **4c** are found as 2.82, 2.77 and 2.72 eV

Table 2 Optimized geometrical parameters of **4c** by DFT B3LYP/6–31 + G(d)

Bond Length	Values A°	Bond angle	Values (deg)	Dihedral angle	Values (deg)
N29-C30	1.4584	**C11-N29-C30**	125.70	**H22-C21-C19-H20**	179.85
N29-C11	1.3867	**Cl28-C27-C13**	119.42	**S64-C56-C49-C61**	179.79
C13-C27	1.4665	**S64-C56-C49**	121.77	**N63-C56-C49-C21**	179.39
C27-Cl28	1.7668	**N63-C56-C49**	122.95	**N29-C30-C33-C36**	180.00
C19-C21	1.4280	**C56-C49-C61**	116.17		
C49-C61	1.4347				
C61-N62	1.1636				
C49-C56	1.4592				
C56-N63	1.3001				
C56-S64	1.7894				
C12-H16	1.0842				
C19-H20	1.0859				
C30-H31	1.0959				

respectively in Fig. 9. The smallest energy gap values (2.72 eV) of **4c**, in comparison with **4a** and **4b**, mainly owing to the reduced LUMO energy as the result of the insertion of 2-(benzothiazol-2-yl) cyanomethylene as an electron acceptor. The results indicate that increasing the electron-accepting capacity of the acceptors can reduce the band gaps.

Molecular Electrostatic Potential Surface (MEPs)

The effect of D-A groups was examined by observing the various H and L levels and the MEPs at the B3LYP/6–31 + G(d) optimized geometry of **4a-4c (**Fig. 8**)**. The charge distributions helps to understand the dye interaction with another one which is valuable to describe the sites of "electrophilicity" and nucleophilic reactions [80, 81]. The potential values defined by different colours reduces as follows: blue> orange> red [82]. Negative – low potentials in MEPs represent the abundance of electrons while positive – high potentials represent an absence of electrons. A deep red colour was used to denote the negative – low potentials and the positive – high potentials was represented by a deep blue colour. The negative (red) low potentials are found noticeably in the region of the

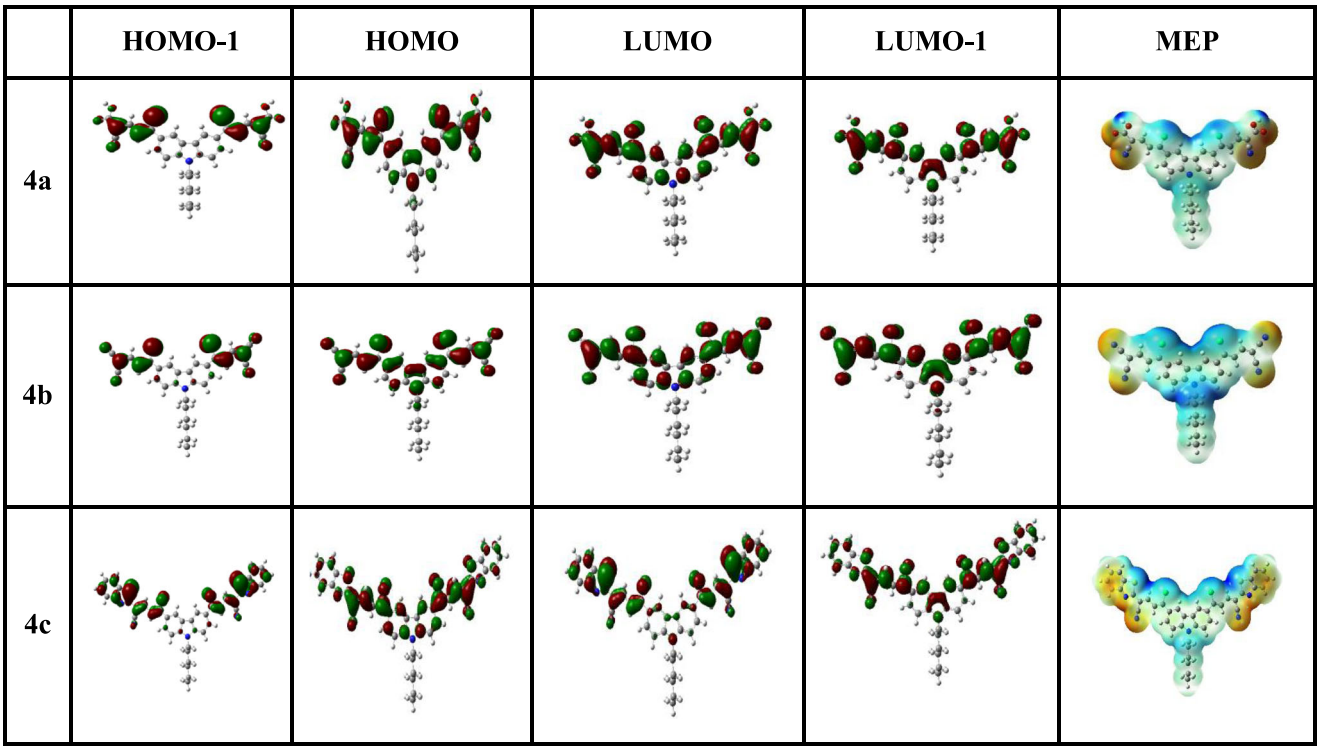

Fig. 8 Frontier molecular orbitals and MEP diagram of **4a-4c** obtained at B3LYP/6–31 + G(d) level

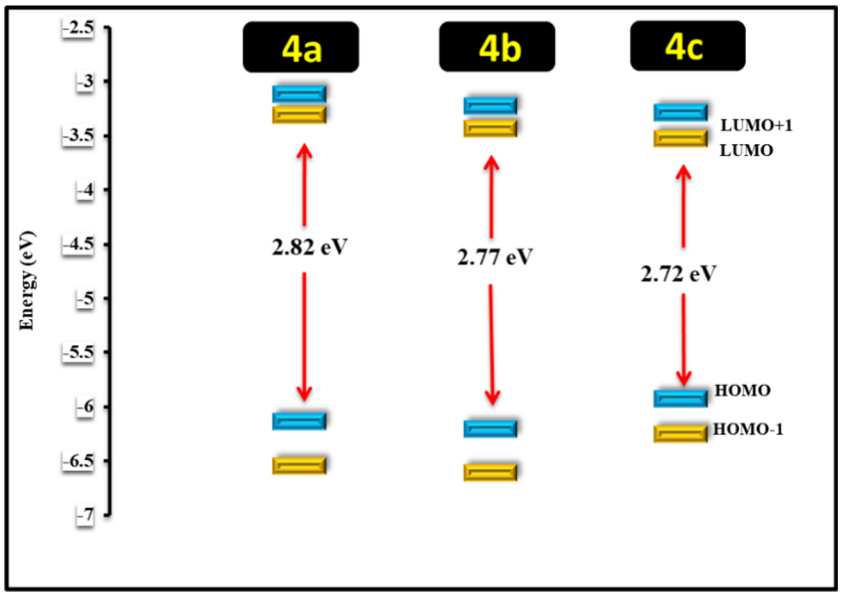

Fig. 9 HOMO-LUMO band gap diagram of **4a-4c** in chloroform

anchoring group and the positive (blue) high potentials in the donor carbazole and hexyl regions. In the case of **4c**, blue colour is spread over carbazole showing positive low potential and the red colour is mainly dispersed on 2-(benzothiazol-2-yl) cyanomethylene unit showing negative low potential. Similar observations were seen in the case of **4a** and **4b**. From MEPS plots with total SCF density [isovalue = 0.0004 a.u.;(mapped with ESP)] represented total densities for **4a-4c** as ±0.103, ±0.092 and ± 0.111 a.u. respectively.

Global Reactivity Descriptors

The global reactivity parameters electronegativity (χ), hardness (η), softness (S) [83] and electrophilicity index (ω) [84, 85] were estimated using DFT method with the help of H-L gap and all the values are given in Table 3.

Chemical hardness value helps to understand chemical softness of the molecule.

Larger HOMO-LUMO gap signifies the more hardness of the molecule. It can be established that smaller H– > L energy gap results into more softness. Chemical potential (μ) is related to the CT from higher to a lower chemical potential system [86].

A molecule with higher softness value gives lower value of η which shows more reactivity The chemical hardness of the molecule is related to the stability of the molecules [88]. The electrophilicity index estimates the energy lowering of a substance owing to the electron transfer from D to A [87].

The H-L energies give an idea about the electron donating and withdrawing capacity of the molecule which is convenient to evaluate molecular electronic properties. All the equations for calculating global reactivity parameters are given in the supporting information.

Table 3 Chemical reactivity description (eV) for dye **4a-4c**

Dye	HOMO	LUMO	μ[a]	η[b]	ω[c]	S[d]
4a	−6.1364	−3.3129	−4.7247	1.4117	7.9062	0.7083
4b	−6.2050	−3.4335	−4.8192	1.3857	8.3801	0.7216
4c	−6.2567	−3.5312	−4.8939	1.3627	8.7877	0.7338

[a] Chemical potential

[b] hardness of molecule

[c] Global electrophilicity index

[d] Softness of molecule

NLO Properties

Conjugated D-π-A compounds design are recognized to possess high "first hyperpolarizability (β)" value. "Sophisticated and expensive electric Field Induced Second Harmonic Generation" (EFISH) technique is usually used to evaluate the experimental NLO characters [89]. Apart from this, experimental method and DFT computational method are primarily used to furnish a primary understanding of NLO characteristics from spectroscopic and computations data. In view of this, we have used the spectroscopic method and computational method to study the NLO characters of synthesized dyes. Urea is used as a reference for comparison of NLO response of the molecule [90, 91].

NLO Properties Obtained from Experimental Solvatochromic Method

"Mean polarizability" (α_{CT}), "static first hyperpolarizability" (β) and "second hyperpolarizability" (γ) for the dyes **4a-4c** were estimated using the equations given in the SI [92–100]

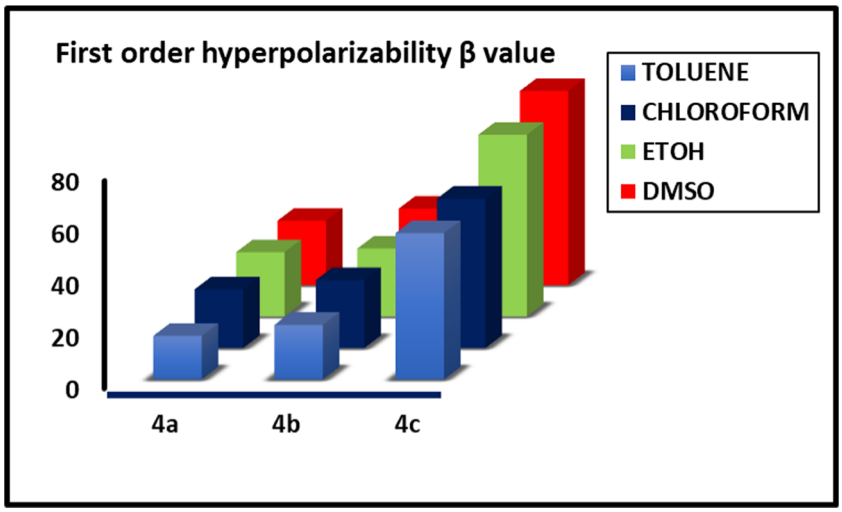

Fig. 10 Solvatochromic β value of **4a-4c** in solvents

and are recorded in Table S7. Among dyes **4a-4c**, hyperpolarizability value rises with the increasing strength of relative donor and acceptor chromophore. Dyes **4a-4c** showed maximum α_{CT} in polar solvent DMSO and minimum α_{CT} in non-polar solvent toluene. **4c** exhibited higher α_{CT} values in DMSO (44.44×10^{-24} esu). Similar observations were obtained for **4a-4c** (Table S7). The order of α_{CT} for the synthesized styryl is as **4c > 4b > 4a**. The trend gives an idea about the strength of acceptors and the length of π-delocalization in styryl molecules. The hyperpolarizability (β) was estimated using "two-level microscopic model" based on Oudar [101, 102] equation in different solvents. β value for **4a** (16.74×10^{-30} esu), **4b** (20.93×10^{-30} esu) and **4c** (56.22×10^{-30} esu) respectively in toluene while **4a** (24.81×10^{-30} esu), **4b** (29.45×10^{-30} esu), **4c** (74.74×10^{-30} esu) respectively in DMSO. The order of β value for dyes is found as **4c > 4b > 4a**. β value is found to be maximum in polar solvents for dyes **4a-4c**. These molecules exhibited higher "hyperpolarizability" (β) values than urea (0.371×10^{-30} esu). The "three-level model" is applied to calculate "second order hyperpolarizability" (γ) at molecular level initiating from the electronic polarization [103, 104]. The value of $\langle\gamma\rangle$ for **4b** and **4c** is larger than **4a** which suggest the higher electron accepting capacity of dicyanovinyl and benzthiazole group.

NLO Values Obtained from Computational Methods

Theoretical method was also used to study the NLO properties. The, a_0, β_o, γ for **4a**, **4b**, and **4c** was calculated using B3LYP/6–31 + G (d) and CAM- B3LYP/6–31 + G (d) basis set (Table S8). It is clear from the observations that a_0 and β_0

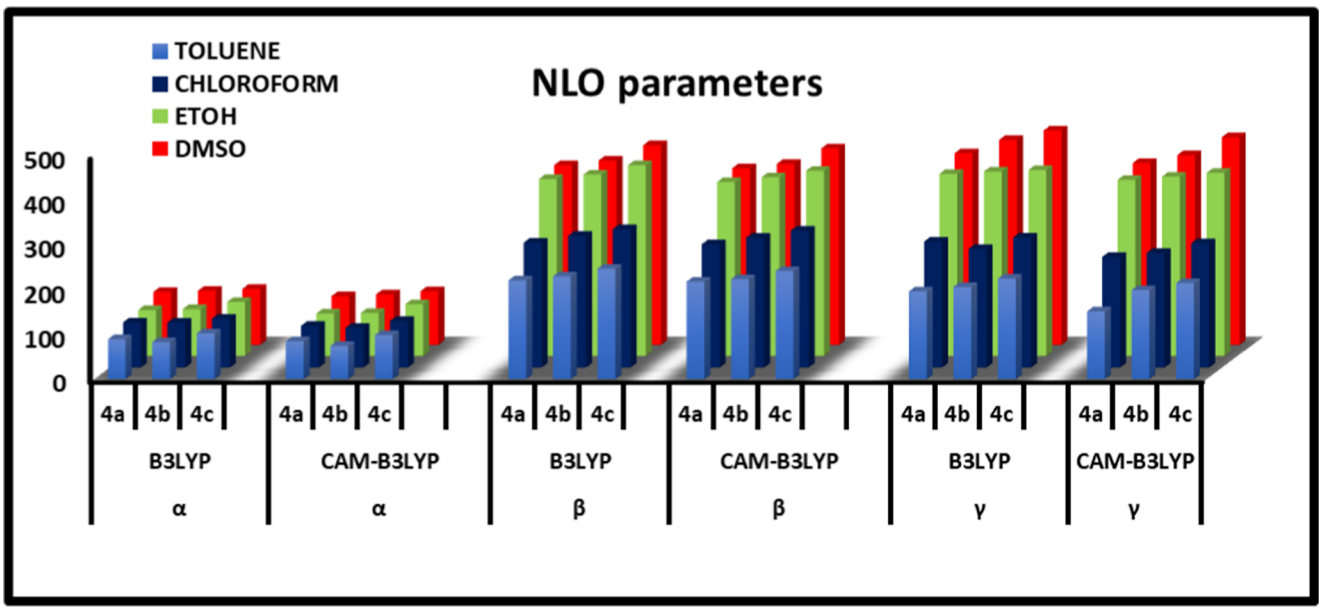

Fig. 11 Computational a_0, β_o, γ values of **4a-4c** in different solvents

values for **4a-4c** are smaller in a non-polar solvent whereas higher in a polar solvent. **4c** exhibited a smaller value of α_0 at (103.58×10^{-24} esu) in toluene and higher at (125.19×10^{-24} esu) in DMSO by using B3LYP basis set and α_0 at (99.34×10^{-24} esu) in toluene and (119.95×10^{-24} esu) in DMSO by CAM-B3LYP basis set. The computed β_0 of **4c** using CAM-B3LYP basis set is (242.46×10^{-30} esu) in toluene and (439.62×10^{-30} esu in DMSO) and computed β_0 of **4b** (224.23×10^{-30} esu) in toluene and (404.79×10^{-30} esu in DMSO). The higher value of β_0 in polar solvent shows strong solute-solvent interaction. γ values using CAM-B3LYP for **4c** in toluene is (215.42×10^{-36} esu) and (464.62×10^{-36} esu) in DMSO. Similar results were given by **4a** and **4b**. These values are larger as compared to urea (0.68×10^{-36} esu). NLO response can be associated with the H-L energy gap. The calculated energy gaps were observed between 2.72–2.82 eV which is smaller as compared to urea ($\Delta E = 6.7063$ eV).

The trend of a_0, β_0 and γ value is found to be as **4c > 4b > 4a**. Overall calculations of NLO parameters shows that **4c** possess better strength of acceptors and the length of π-delocalization compared to **4a** and **4b**. The long range-separated hybrid CAM-B3LYP performed well compared to B3LYP for NLO properties and results are found to be in good contract with experimental results. From the spectroscopic and DFT observations, it can be concluded that accepting capacity of anchoring group and extended π-conjugation are the key points to increase NLO properties of the dyes (Figs. 10 and 11).

Conclusion

In summary, we have reported a series of A-π-D-π-A molecules using carbazole as a donor and three different acceptors of varying withdrawing capacity. Solvatochromism data showed that the synthesized styryl **4c** show slightly red shifted emission compared to **4a**, **4b, R2** and reported carbazole styryls (**R1**) owing to the strong acceptor, extended π-conjugation and assistance of extra electron withdrawing chlorine group in conjugation. The chemical structure of dyes with extended π-delocalization in the molecules are responsible for FMRs which leads to enhanced emission intensity. Compounds **4a-4c** were found to show viscosity dependent properties in which **4c** showed a higher response. This shows that reported styryls can be used as excellent FMRs for the viscosity measurements.

Further, we have studied the AEE phenomenon of **4a-4c**. All the three dyes were found to be AEE-active in DMF-H_2O mixture and emit bright orange luminescence under UV light. From the investigation, we confirm that optical properties of molecules can be modified by extending conjugation, introducing longer alkyl chain, inserting electronegative groups like chlorine and varying electron accepting groups in the design of a molecule. So, the present research may provide suitable enlightenment for the future design of FMR material and AEE active molecules. DFT and TD-DFT computations were done to find out the computed vertical excitation which showed consistency with the experimental values. The NLO character are studied using solvatochromic and computational methods, global hybrid "B3LYP" and range separated "CAM-B3LYP" method where, CAM-B3LYP results are found to be more consistent. Thus, the synthesized push-pull chromophores based on carbazole dyes can be served as a good candidate of NLO material with good β_o values.

Acknowledgments The author, Prerana Kumar Lokhande is thankful to University Grants Commission (Greentech), New Delhi (India) for the award of Junior and Senior Research fellowships.

Compliance with Ethical Standards

Conflict of Interest There are no conflicts to declare.

References

1. Brunner K, van Dijken A, B€orner H, Bastiaansen JJ, Kiggen NMM, Langeveld BMW (2004) J Am Chem Soc 126:6035–6042
2. Chu H-C, Sahu D, Hsu Y-C, Padhy H, Patra D, Lin J-T (2012) Structural planarity and conjugation effects of novel symmetrical acceptor–donor–acceptor organic sensitizers on dye-sensitized solar cells. Dyes Pigments 93:1488–1497
3. Ning Z, Zhang Q, Wu W, Pei H, Liu B, Tian H (2008) Starburst Triarylamine Based Dyes for Efficient Dye-Sensitized Solar Cells. J Org Chem 73:3791–3797
4. Yoon KR, Ko S-O, Lee SM, Lee H (2007) Synthesis and characterization of carbazole derived nonlinear optical dyes. Dyes Pigments 75:567–573
5. Pacansky J, Waltman RJ (1992) X-ray photoelectron and optical absorption spectroscopic studies on the dye chlorodiane blue, used as a carrier generation molecule in organic photoconductors. J Am Chem Soc 114:5813–5839
6. Mor GK, Basham J, Paulose M, Kim S, Varghese OK, Vaish A (2010) High-Efficiency Förster Resonance Energy Transfer in Solid-State Dye Sensitized Solar Cells. Nano Lett 10:2387–2394
7. Yang Z, Zhao N, Sun Y, Miao F, Liu Y, Liu X (2012) Highly selective red- and green-emitting two-photon fluorescent probes for cysteine detection and their bio-imaging in living cells. Chem CommunCamb 48:3442–3444
8. Meerholz K, Volodin BL, Sandalphon N, Kippelen K, Peyghambarian N (1994) A photorefractive polymer with high optical gain and diffraction efficiency near 100%. Nature 371: 497–500
9. Cox AM, Blackburn RD, West DP, King TA, Wade FA, Leigh DA (1996) Crystallization-resistant photorefractive polymer composite with high diffraction efficiency and reproducibility. Appl Phys Lett 68:2801–2803
10. Gupta VD, Padalkar VS, Phatangare KR, Patil VS, Umape PG, Sekar N (2011) The synthesis and photo-physical properties of extended styryl fluorescent derivatives of N-ethyl carbazole. Dyes Pigments 88:378–384
11. Gupta VD, Tathe AB, Padalkar VS, Umape PG, Sekar N (2013) Red emitting solid state fluorescent triphenylamine dyes:

Synthesis, photo-physical property and DFT study. Dyes Pigments 97:429–439
12. Law KY (1993) Organic photoconductive materials: recent trends and developments. Chem Rev 93:449–486
13. Yang MJ, Tsutsui T (2000) Jpn J Appl Phys 39:1828
14. Luo J, Xie Z, Lam JWY, Cheng L, Chen H, Qiu C, Kwok HS, Zhan X, Liu Y, Zhu D, Tang BZ (2001) Aggregation-induced emission of 1-methyl-1,2,3,4,5-pentaphenylsilole. Chem Commun:1740–1741
15. Yang Z, Qin W, Lam JWY, Chen S, Sung HHY, Williams ID, Tang BZ (2013) Fluorescent pH sensor constructed from a heteroatom-containing luminogen with tunable AIE and ICT characteristics. Chem Sci 4:3725
16. Roy S, Stollberg P, Herbst-Irmer R, Stalke D, Andrada DM, Frenking G, Roesky HW (2015) Carbene-Dichlorosilylene Stabilized Phosphinidenes Exhibiting Strong Intramolecular Charge Transfer Transition. J Am Chem Soc 137:150–153
17. Hong Y, Lam JW, Tang BZ (2011) Aggregation-induced emission. Chem Soc Rev 40:5361–5388
18. Sharma S, Dhir A, Pradeep CP (2014) ESIPT induced AIEE active material for recognition of 2-thiobarbituric acid. Sens Actuators B Chem 191:445–449
19. An BK, Kwon SK, Jung SD, Park SY (2002) Enhanced Emission and Its Switching in Fluorescent Organic Nanoparticles. J.Am.Chem.Soc. 124:14410–14415
20. Hu R, Lager E, Aguilar Aguilar A, Liu J, Lam JWY, Sung HHY, Williams ID, Zhong Y, Wong KS, Peña-Cabrera E, Tang BZ (2009) Twisted Intramolecular Charge Transfer and Aggregation-Induced Emission of BODIPY Derivatives. J Phys Chem C 113:15845–15853
21. Liu Y, Tao X, Wang F, Shi J, Sun J, Yu W, Ren Y, Zou D, Jiang M (2007) J Phys Chem C111:6544
22. Wu QY, Peng Q, Niu YL, Gao X, Shuai ZG (2012) Theoretical Insights into the Aggregation-Induced Emission by Hydrogen Bonding: A QM/MM Study. J.Phys.Chem. A116 116:3881–3888
23. Xiao S, Zou Y, Wu J, Zhou Y, Yi T, Li F, Huang CJ (2007) Hydrogen bonding assisted switchable fluorescence in self-assembled complexes containing diarylethene: controllable fluorescent emission in the solid state. Mater.Chem. 17:2483
24. Zhou T, Li F, Fan Y, Song W, Mu X, Zhang H, Wang Y (2009) Hydrogen-bonded dimer stacking induced emission of aminobenzoic acid compounds. Chem.Commun.:3199–3201
25. Deligeorgiev T, Vasilev A (2010) Chemistry F. ColorTechnol:55–80
26. Tokar VP, Losytskyy MY, Ohulchanskyy TY (2010) Styryl Dyes as Two-Photon Excited Fluorescent Probes for DNA Detection and Two-Photon Laser Scanning Fluorescence Microscopy of Living Cells. J Fluoresc 20:865–872
27. Wandelt B, Mielniczak A, Turkewitsch P, Darling GD, Stranix BRS (2003) Substituted 4-[4-(dimethylamino)styryl]pyridinium salt as a fluorescent probe for cell microviscosity. BiosensBioelectron 18:465–471
28. Ismail L (2012) Photophysical properties of a surfactive long-chain styryl merocyanine dye as fluorescent probe. F MJ Lumin 132:2512–2520
29. Horiguchi E, Kitaguchi T, Matsui M (2006) Substituent effects of 2,3-dicyano-5-[4-(diethylamino)styryl]-7-methyl-6H-1,4-diazepines on their use as red dopants in single-layer organic electroluminescence devices. Dyes Pigments 70:43–47
30. Rodrigues CAB, Mariz IFA, Maçoas EMS, Afonso CAM, Martinho JMG (2012) Two-photon absorption properties of push–pull oxazolones derivatives. Dyes Pigments 95:713–722
31. Chan CYK, Lam JWY, Zhao Z, Chen S, Lu P, Sung HHY (2014) Aggregation-induced emission, mechanochromism and blue electroluminescence of carbazole and triphenylamine-substituted ethenes. J Mater Chem C 2:4320–4327
32. Carda-Moreno I, Costela A, Mantin V, Pintado-Sierra M, Sastre R (2009) Materials for a Reliable Solid-State Dye Laser at the Red Spectral Edge. Adv Funct Mater 19:2547–254752
33. Patel DG, Bastianon NM, Tongwa P, Leger JM, Timofeeva TV, Bartholomew GP (2011) Modification of nonlinear optical dyes for dye sensitized solar cells: a new use for a familiar acceptor. J Mater Chem 21:4242
34. Slama-Schwok MB-DA, Lehn J-M (1990) Intramolecular charge transfer in donor-acceptor molecules. J Phys Chem 94:3894–3902
35. Han F, Zhang R, Zhang Z, Su J, Ni Z (2016) A new TICT and AIE-active tetraphenylethene-based Schiff base with reversible piezofluorochromism. RSC Adv 6:68178–68184
36. Zhang Y, Wang J-H, Zheng J, Li D (2015) A Br-substituted phenanthroimidazole derivative with aggregation induced emission from intermolecular halogen–hydrogen interactions. Chem Commun 51:6350–6353
37. Dalton LR, Benight SJ, Johnson LE, Knorr DB, Kosilkin I, Eichinger BE (2011) Systematic Nanoengineering of Soft Matter Organic Electro-optic Materials†. Chem Mater 23:430–445
38. Lupo D (1995) Molecular nonlinear optics: materials, physics, and devices. Edited by J. Zyss, academic press, San Diego. CA 1994, XIII, 478 pp., hardcover, ISBN 0-12- 784450-3. Adv Mater 7: 248–249
39. Dalton LR, Sullivan PA, Bale DH (2010) Electric Field Poled Organic Electro-optic Materials: State of the Art and Future Prospects. Chem Rev 110:25–25
40. Cole JM (2003) Organic materials for second-harmonic generation: advances in relating structure to function. Trans Roy Soc A: Math Phys Eng Sci 361:2751–2770
41. Kanis DR, Ratner MA, Marks TJ (1994) Design and construction of molecular assemblies with large second-order optical nonlinearities. Quantum chemical aspects. Chem Rev 94:195–242
42. S.R. Forrest. M.E (2007) Introduction: Organic Electronics and Optoelectronics. Chem Rev 107:923–925
43. Thomas KRJ, Lin JT, Tao Y-T, Ko C-W (2000) Novel Green Light-Emitting Carbazole Derivatives: Potential Electroluminescent Materials. Adv Mater 12:1949–1951
44. Ciorba S, Galiazzo G, Mazzucato U, Spalletti A (2010) Photobehavior of the Geometrical Isomers of Two 1,4-Distyrylbenzene Analogues with Side Groups of Different Electron Donor/Acceptor Character. J Phys Chem A 114: 10761–10768
45. Sagara Y, Kato T (2009) Nat Chem 1:1605
46. Sagara Y, Kato T (2011) Angew Chem 123:9294
47. Nagura K, Saito S, Yusa H, Yamawaki H, Fujihisa H, Sato H, Yamaguchi YS aS (2013) Distinct Responses to Mechanical Grinding and Hydrostatic Pressure in Luminescent Chromism of Tetrathiazolylthiophene. J Am Chem Soc 135:10322–10325
48. Kumbhar HS, Deshpande SS, Shankarling GS (2016) Chemistry Select 1:2058–2064
49. Thorat KG, Kamble P, Mallah R, Ray AK, Sekar N (2015) Congeners of Pyrromethene-567 Dye: Perspectives from Synthesis, Photophysics, Photostability, Laser, and TD-DFT Theory. J Org Chem 80:6152–6164
50. Thorat KG, Bhakhoa H, Ramasami P, Sekar N (2015) NIR-Emitting Boradiazaindacene Fluorophores -TD-DFT Studies on Electronic Structure and Photophysical Properties. J Fluoresc 25: 69–78
51. Shen J, Snook RD (1989) Thermal lens measurement of absolute quantum yields using quenched fluorescent samples as references. Chem Phys Lett 155:583–586
52. Ooyama Y, Nagano T, Inoue S, Imae I, Komaguchi K, Ohshita J, Harima Y (2011) Dye-Sensitized Solar Cells Based on Donor-π-Acceptor Fluorescent Dyes with a Pyridine Ring as an Electron-Withdrawing-Injecting Anchoring Group. Chem-Eur J 17:14837–14843

53. Zhao J, Yang X, Cheng M, Li S, Sun L (2013) Molecular Design and Performance of Hydroxylpyridium Sensitizers for Dye-Sensitized Solar Cells. ACS Appl Mater Interfaces 5:5227–5231
54. Sacconi L (1966) Tetrahedral complexes of nickel(II) and copper(II) with schiff bases. Coord Chem Rev 1:126–132
55. Yamada S (1966) Recent aspects of the stereochemistry of schiff-base-metal complexes. Coord Chem Rev 1:415–437
56. Mehrotra C, Srivastva G, Saraswat BS (1982) Rev Silicon, Germanium, Tin, Lead Compd 6:171
57. Nath M, Goyal S (1995) Main Group Met Chem 19:75
58. Siddiqui HL, Iqbal A, Ahmad S, Weaver GW (2006) Synthesis and Spectroscopic Studies of New Schiff Bases. Molecules 11: 206–211
59. G.E.M.J.F.G.W.T. H. B. Schlegel, G.A.S.M.A.R.J.R.C.G.S.V.B. B. Mennucci, J.P.H.N.M.C.X.L.H.P.H. A. F. Izmaylov, J.B.G.Z.J.L.S.M.H.M.E.K.T. R. Fukuda, J.A.H.M.I.T.N.Y.H.O.K.H.N. T. Vreven, K.N.M.J.J.E.P.F.O.M.B.J.J.H. E. Brothers, J.K.V.N.S.R.K.J.N.K.R. A. Rendell, J.E.C.B.S.S.I.J.T.M.C.N.R.J.M.M. M. Klene, R.E.S.K.J.B.C.V.B.C.A.J.J. R. Gomperts, K.O.Y.A.J.A.R.C.C.P.J.W.O. R. L. Martin, S.M.V.G.Z.G.A.V.P.S. J. J. Dannenberg, and D.D.A.D.D.O.F.J.B.F.J.V.O. J. Cioslowski, W.C.J.F.G. Inc., Gaussian 09, Revision A.1, (n.d.)
60. Gao BR, Wang HY, Hao YW, Fu LM, Fang HH, Jiang Y, Wang L, Chen QD, Xia H, Pan LY, Ma YG, Sun HB (2010) Time-Resolved Fluorescence Study of Aggregation-Induced Emission Enhancement by Restriction of Intramolecular Charge Transfer State. J Phys Chem B 114:128–134
61. Al-Sabtl KEA (1983) M J Phys Chem 87:446
62. Lai C-T, Hong J-L (2010) Aggregation-Induced Emission in Tetraphenylthiophene-Derived Organic Molecules and Vinyl Polymer. J Phys Chem B 114:10302–10310
63. Chen M, Li L, Nie H, Tong J, Yan L, Xu B, Sun JZ, Tian W, Zhao Z, Qin A, Tang BZ (2015) Tetraphenylpyrazine-based AIEgens: facile preparation and tunable light emission. Chem Sci 6:1932–1937
64. Bruni S, Cariati E, Cariati F, Porta FA, Quici S, Roberto D (2001) Determination of the quadratic hyperpolarizability of trans-4-[4-(dimethylamino)styryl]pyridine and 5-dimethylamino-1,10-phenanthroline from solvatochromism of absorption and fluorescence spectra: a comparison with the electric-field-induced second-harmonic generation technique. Spectrochim Acta Part A Mol BiomolSpectrosc 57:1417–1426
65. Coe BJ, Harris JA, Asselberghs I, Clays K, Olbrechts G, Persoons A (2002) Quadratic Nonlinear Optical Properties ofN-Aryl Stilbazolium Dyes. Adv Funct Mater 12:110–116
66. Kawski A (2002) Zeitschrift Fur Naturforsch - Sect A. J Phys Sci 57:255–262
67. Chamma A, Viallet PCR (1970) Acad Sci Paris Ser C 270:1901–1904
68. Kawski A (1964) Dipolmomenteeiniger Naphtholeim Grundund Anregungszust and. Naturwissenschaften. 51:82–83
69. Rettig W (1986) Ladungstrennung in angeregten Zuständen entkoppelter Systeme – TICT-Verbindungen und Implikationen für die Entwicklung neuer Laserfarbstoffe sowie für den Primärprozeß von Sehvorgang und Photosynthese. AngewChem. 98:969–986
70. Valeur B (2001) Related titles from WILEY-VCH analytical atomic spectrometry with flames and plasmas handbook of analytical techniques single-molecule detection in solution. Methods and Applications 8
71. McRae EG (1954) J Phys Chem 6:1957
72. Eisenthal KB, Rieckhoff KE (1971) Polarizability of Molecules in Excited Electronic States. J Chem Phys 55:3317–3327
73. Coe BJ, Harris JA, Asselberghs I, Clays K, Olbrechts G, Persoons A (2002) Quadratic Nonlinear Optical Properties ofN-Aryl Stilbazolium Dyes. Adv Funct Mater 12:110–116
74. Beens H, Knibbe H, Weller A (1967) Dipolar nature of molecular complexes formedin the excited state. J Chem Phys 47:1183–1184
75. Zheng J, Kang YK, Therien MJ, Beratan DN (2005) Generalized Mulliken−Hush Analysis of Electronic Coupling Interactions in Compressed π-Stacked Porphyrin−Bridge−Quinone Systems. J Am Chem Soc 127:11303–11310
76. Zheng J, Kang YK, Therien MJ, Beratan DN (2005) Generalized Mulliken−Hush Analysis of Electronic Coupling Interactions in Compressed π-Stacked Porphyrin−Bridge−Quinone Systems. J Am Chem Soc 127:11303–11310
77. Kadam MML, Patil DS, Sekar N (2019) Red emitting coumarin based 4, 6-disubstituted-3-cyano-2-pyridones dyes – Synthesis, solvatochromism, linear and non-linear optical properties. J Mol Liq 276:385–398
78. Li J, Zhang Y, Mei J, Lam JWY, Hao J, Tang BZ (2015) Aggregation-Induced Emission Rotors: Rational Design and Tunable Stimuli Response. Chem - A Eur J 21:907–914
79. Zhao Z, Lam JWY, Tang BZ (2012) Tetraphenylethene: a versatile AIE building block for the construction of efficient luminescent materials for organic light-emitting diodes. J Mater Chem 22: 23726
80. Alam MJ, Ahmad S (2012) Anharmonic vibrational studies of l-aspartic acid using HF and DFT calculations. Spectrochim Acta - Part A Mol Biomol Spectrosc 96:992–1004
81. Uludağ N, Serdaroğlu G, Yinanc A (2018) A novel synthesis of octahydropyrido[3,2-]carbazole framework of aspidospermidine alkaloids and a combined computational, FT-IR, NMR, NBO, NLO, FMO, MEP study of the cis-4a-Ethyl-1-(2hydroxyethyl)-2,3,4,4a,5,6,7,11c-octahydro-1H-pyrido[3,2-c]carbazole. J Mol Struct 1161:152–168
82. Thul P, Gupta VP, Ram VJ (2010) Structural and spectroscopic studies on 2-pyranones. P Tandon Spectrochim Acta - Part A Mol Biomol Spectrosc 75:251–260
83. Yang W, Parr RG (1985) Hardness, softness, and the fukui function in the electronic theory of metals and catalysis. Proc Natl Acad Sci 82:6723–6726
84. Parr RG, Szentpály LV, Liu S (1999) Electrophilicity Index. J Am Chem Soc 121:1922–1924
85. Koopmans T (1934) Über die Zuordnung von Wellenfunktionen und Eigenwerten zu den Einzelnen Elektronen Eines Atoms. Physica. 1:104–113
86. Parr RG, Pearson RG (1983) Absolute hardness: companion parameter to absolute electronegativity. J Am Chem Soc 105:7512–7516
87. Rezende MC, Dominguez M, Aracena A, Millán D (2011) Solvatochromism and electrophilicity. Chem Phys Lett 514:267–273
88. Pearson RG (1985) Absolute electronegativity and absolute hardness of Lewis acids and bases. J Am Chem Soc 107:6801–6806
89. Jiao Z (2011) N, Huang, K W, Wang, P, Wu J Org Lett 13:3652–3655
90. Katariya S, Rhyman L, Alswaidan IA, Ramasami P, Sekar N (2017) Triphenylamine-Based Fluorescent Styryl Dyes: DFT, TD-DFT and Non-Linear Optical Property Study. J Fluoresc 27: 993–1007
91. Margar SN, Sekar N (2016) Nonlinear optical properties of curcumin: solvatochromism-based approach and computational study. Mol Phys 114:1867–1879
92. Cho MJ, Choi DH, Sullivan PA, Akelaitis AJP, Dalton LR (2008) Recent progress in second-order nonlinear optical polymers and dendrimers. Prog Polym Sci 33:1013–1058
93. Tayade RP, Sekar N (2016) Benzimidazole-thiazole based NLOphoric styryl dyes with solid state emission – Synthesis,

photophysical, hyperpolarizability and TD-DFT studies. Dyes Pigments 128:111–123
94. Jenekhe SA, Osaheni JA, Meth JS, Vanherzeele H (1992) Nonlinear optical properties of poly(p-phenylenebenzobisoxazole). Chem Mater 4:683–687
95. Oudar JL, Chemla DS (1977) Hyperpolarizabilities of the nitroanilines and their relations to the excited state dipole moment. J Chem Phys 66:2664–2668
96. Momicchioli F, Ponterini G, Vanossi D (2008) First- and Second-Order Polarizabilities of Simple Merocyanines. An Experimental and Theoretical Reassessment of the Two-Level Model. J Phys Chem A 112:11861–11872
97. Meyers F, Marder SR, Pierce BM, Bredas JL (1994) Electric Field Modulated Nonlinear Optical Properties of Donor-Acceptor Polyenes: Sum-Over-States Investigation of the Relationship between Molecular Polarizabilities (.alpha., .beta., and .gamma.) and Bond Length Alternation. J Am Chem Soc 116:10703–10714
98. S.K. Lanke, N. Sekar, J. Fluoresc. 25(2015)1469–1480. J.L. Oudar, D.S. Chemla, J. Chem. Phys. 66, (1977), 2664–2668
99. Abbotto A, Beverina L, Bradamante S, Facchetti A, Klein C, Pagani GA et al (2003) Chem Eur J 9:991–2007
100. Momicchioli F, Ponterini G, Vanossi D (2008) First- and second-order polarizabilities of simple merocyanines. J Phys Chem A 112: 11861–11872
101. Oudar JL (1977) Optical nonlinearities of conjugated molecules. Stilbene derivatives and highly polar aromatic compounds. J Chem Phys 67:446–457
102. Margar SN, Rhyman L, Ramasami P, Sekar N (2016) Fluorescent difluoroboron-curcumin analogs: An investigation of the electronic structures and photophysical properties. Spectrochim Acta Part A Mol Biomol Spectrosc 152:241–251
103. Champagne B, Perpete EA, Andre J, Kirtman B (1997) Analysis of the vibrational static and dynamic second hyperpolarizabilities of polyacetylene chains. Syn Metals 85:1047–1050
104. Parr RG, Yang W Density-functional theory of atoms and molecules. Oxford University Press, New York, p 19
105. Kremser G, Hofmann OT, Sax S, Kappaun S, List EJW, Zojer E, Slugovc C (2008) Synthesis and Photophysical Properties of 3,6-Diphenyl-9-hexyl-9H-carbazole Derivatives Bearing Electron Withdrawing Groups. Monatsh Chem 139:223–231
106. Lanke SK, Sekar N (2016) Novel NLOphoric 2-methoxy carbazole-based push pull chromophores: Synthesis, photophysical properties and TD-DFT Study. J Photochem Photobiol A Chem 321:63–71